An Eddy-Diffusivity Mass-Flux Parameterization for Modeling Oceanic Convection

Hervé Giordani, Romain Bourdallé-Badie, Gurvan Madec

HAL Id: insu-03668360
https://insu.hal.science/insu-03668360

Submitted on 15 May 2022

An Eddy-Diffusivity Mass-Flux Parameterization for Modeling Oceanic Convection

Hervé Giordani[1], **Romain Bourdallé-Badie[2]**, and **Gurvan Madec[3]**

[1]CNRM/CNRS, UMR-3589, Météo-France, Toulouse, France, [2]Mercator Ocean International, Ramonville, France, [3]Sorbonne Universités, UPMC, Paris, France

Abstract A new one-dimensional (1-D) parameterization of penetrative convection has been developed in order to have a better representation of the vertical mixing in ocean general circulation models. Our approach is inspired from atmospheric parameterizations of shallow convection which assumes that in the convective boundary layer, the subgrid-scale fluxes result from two different mixing scales: small eddies, which are represented by an Eddy-Diffusivity (ED) contribution, and large eddies associated with thermals, which are represented by a mass-flux contribution. In the present work, the local (small eddies) and nonlocal (large eddies) contributions are unified into an Eddy-Diffusivity-Mass-Flux (EDMF) parameterization which treats simultaneously the whole vertical mixing. EDMF is implemented in the community ocean model NEMO and tested in its 1-D column version. Deepening of dense water in analytic cases, successfully reproduced in LES simulations, is more realistic with EDMF than with standard diffusion parameterizations. Also the convective events observed in the western Mediterranean at the Lion station and in the North Pacific Ocean at the PAPA station are more realistic in terms of sequencing and amplitude with EDMF.

Plain Language Summary A new representation of oceanic convection has been developed in order to have a better representation of vertical mixing in ocean models. Our proposition is to represent oceanic convection consistently to atmospheric convection. We want to represent the convective plumes in oceans in the same way that the cumulus clouds are represented in the atmosphere. In this unified approach, the oceanic vertical mixing is viewed as a combination of large eddies associated with strong nonbuoyant downdrafts and small eddies which induce local turbulence. This new paradigm of oceanic mixing leads to more realistic simulations of the hydrological properties of water masses. In the future, it is expected to obtain more reliable climate projections.

1. Introduction

The primary role of deep convection is to consume the static instability generated by a surface buoyancy loss or by advection of dense water at any level. The large vertical velocities involved in deep convection play a crucial role in formation of intermediate and mode waters and ultimately in the thermohaline circulations (Martin et al., 2013; Moore et al., 2015; Piron et al., 2016). By controlling the biogeochemical fluxes between the mixed-layer and the ocean interior, the convective velocities are also important in the ocean carbon budget at global scale (Capet et al., 2008; Iudicone et al., 2011; Lapeyre & Klein, 2006; Lévy et al., 2012; Thomas & Ferrari, 2008).

Buoyancy-driven convective vertical velocities occur in localized areas with intensities up to $0.15\,\mathrm{m\,s^{-1}}$ (Gascard, 1991; Marshall & Schott, 1999; Martin et al., 1996) which transport water over several hundred meters during short periods (in the order of hours) (Aagaard & Carmack, 1989). Deep convection spots were identified in the Greenland, Labrador, Irminger, Weddell, and Mediterranean Seas where cross-isopycnal advections control the temperature and salinity vertical structure, the deep water masses properties, and finally the deep circulation.

The traditional way to parameterize vertical turbulent transport in ocean regional models and Ocean General Circulation Models (OGCMs) is through an Eddy-Diffusivity (ED) approach, which is a common local K-theory. The ED method estimates the vertical turbulent flux of a field ψ as $\overline{w'\psi'} = -K_z \frac{\partial \psi}{\partial z}$, where K_z is the ED coefficient and has units of $\mathrm{m^2\,s^{-1}}$. This parameterization implies that the flux $\overline{w'\psi'}$ is down the local

gradient of ψ and is also called small-eddy closure technique. This method succeeds in representing turbulent fluxes and mixed-layer depths for diffusion regimes but fails in representing vertical transports induced by organized large eddies because the parcels move regardless of the local gradient. In particular, K-theory cannot properly describe the downward convection flux particularly in the lower part of the mixed-layer, where often a slightly stable stratification profile is observed. For this reason, K-theory is not recommended for convective mixed layers.

In order to overcome this deficiency, some modifications were introduced into ED formulations to take into account the effects of convective plumes which propagate counter-gradient of the stratification. The first modification introduces a counter-gradient term in the K-theory in order to improve the entrainment process at the mixed-layer base (Deardorff, 1966; Ertel, 1942). This approach, currently used in the KPP (Large et al., 1994) and OSMOSIS (Madec & NEMO System Team, 2016) parameterizations, mimics the nonlocal vertical transport associated with the large eddies which develop in the convective layer. The second modification called Non-Penetrative Convective (NPC) adjustment parameterization (Ilicak et al., 2014; Madec, Chartier, Delecluse, et al., 1991) instantaneously removes the gravitational instability by mixing all tracers over the statically unstable portions until the density structure becomes neutrally stable. This scheme avoids the existence of permanent and unrealistic static instabilities (Killworth, 1989) and was successfully used for deep water formation in the Northwestern Mediterranean Sea (Madec, Chartier, & Crépon, 1991; Madec, Chartier, Delecluse, et al., 1991). The third modification called Enhanced Vertical Diffusion (EVD) parameterization is currently used in the NEMO ocean model and assigns very large values of the vertical eddy mixing coefficient ($K_z = 10\,\mathrm{m}^2\,\mathrm{s}^{-1}$) in regions where the stratification is unstable ($N^2 < 0$ Lazar et al., 1999; Madec & NEMO System Team, 2016). This parameterization is less time consuming than the nonpenetrative convective adjustment algorithm.

Smith (1989) has shown that the thermohaline circulation is sensitive to these convective parameterizations and Holland (1979) has shown the significant sensitivity of climate simulations to several convective adjustment schemes. Skyllingstad et al. (1991) showed that the convective adjustment did not mix enough deep-layers to produce realistic water masses at the right depth in the Labrador Sea. Sander et al. (1995) also concluded that convective adjustment in OCGMs neither produce realistic vertical density structure nor create the correct quantity of deep water. The enhanced vertical diffusivity used in the NEMO model leads to the same discrepancies and also fails in capturing the right timing of the dense water production. Observations (Clarke & Gascard, 1983) have shown that convection penetrates down to 1,500 m in few days in the Labrador Sea while modified ED parameterizations are not appropriate to represent convection because convection is basically an advective process. This points out that convection and diffusion are different physical processes which have to be treated distinctly.

Throughout this study, the so-called eddy-diffusion (ED) scheme chosen is based on a parameterization of the second-order turbulent moments expressed as a function of the Turbulent Kinetic Energy (TKE; 1.5 turbulent closure scheme Gaspar et al., 1990). This parameterization is currently used in applications with the NEMO code (Lellouche et al., 2018; Madec & NEMO System Team, 2016; Reffray et al., 2015) and a recent presentation including the wave-induced terms can be found in Couvelard et al. (2019).

This paper proposes to represent oceanic convection consistently to atmospheric convection. Conceptually this approach aims at taking into account the bulk effect of an ensemble of convective plumes immersed into the environment of a model grid-cell in the tracer equations (Figure 1). Consider that this population of plumes, formed of particles, occupies a fraction of the model grid-cell called convective area as shown on Figure 1. According to this vision, all these particles move in the same way. The particles in the plume, which is represented by a pipe, start moving down because they are denser than their environment. The difference of density between the plume and its environment controls the buoyancy force whose work on the vertical drives the downward velocity of the particles. This process is nonlocal and so-called Mass-Flux (MF) because it is associated with transport on the vertical induced by organized large eddies. When the particles density become lighter than their environment, the buoyancy force reverses and tends to slow down the vertical velocity. The overshooting zone is defined by the first level where the buoyancy force reverses up to the level of no motion. This zone is fully controlled by counter-gradient fluxes.

The diffusion and convection fluxes, namely, the local and nonlocal vertical transports, respectively, are unified into a new single scheme in order to have an appropriate treatment of the vertical mixing in ocean general circulation models. In this approach, the subgrid-scale fluxes result from a combination of small eddies which induce local turbulence and large eddies which are associated with strong nonbuoyant
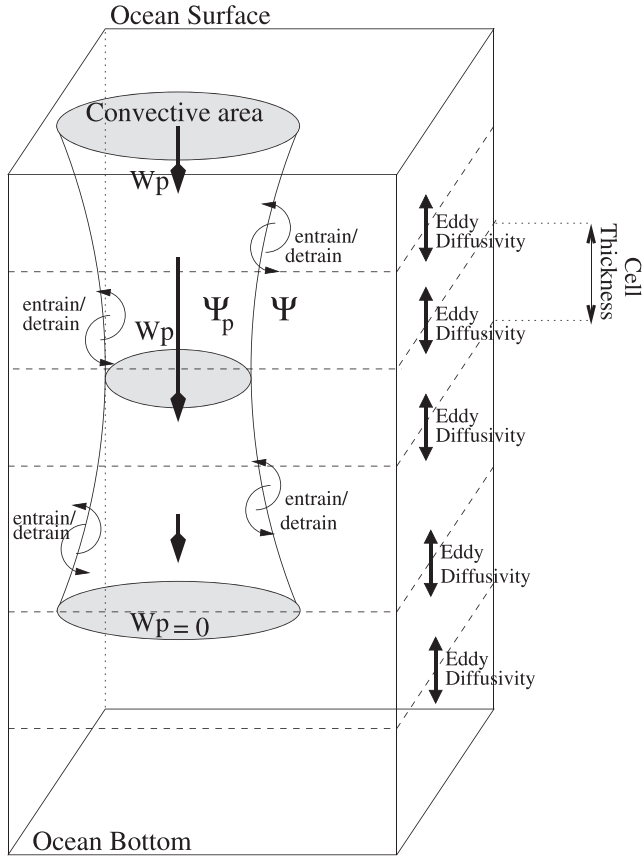
Figure 1. Schematic representation of a convective plume in a single grid-mesh. The plume is represented by a pipe which occupies a fractional convective area of the environment. ψ_p and ψ represent the water properties of the plume and the environment, respectively. W_p is the plume vertical velocity and curly arrows along the plume envelope symbolize the entrainment-detrainment processes. The eddy-diffusive mixing is symbolized by double vertical arrows between two cells.

downdrafts (Siebesma & Cuijpers, 1995; Soares et al., 2004). Small eddy fluxes are represented by an ED parameterization while large eddies fluxes, also called vertical convective fluxes, are represented by our Mass-Flux (MF) parameterization, that is why this unified scheme is named Eddy-Diffusivity-Mass-Flux (EDMF). The EDMF parameterization scheme is implemented into the community ocean model NEMO (Madec & NEMO System Team, 2016).

A first attempt to represent oceanic convection has been done in Paluszkiewicz and Romea (1997) with the Ocean Penetrative Plume Scheme (OPPS) which was derived from the first generation parameterization schemes for deep atmospheric convection (Fritsch & Chappell, 1980; Kuo, 1974) and tested in Stössel et al. (2002). OPPS and EDMF differ conceptually because OPPS returns to the OGCM the area-weighted means of plume and environment variables while EDMF explicitly computes the large-eddy convective fluxes which are taken into account in the OGCM prognostic tracer equations. In that way, OPPS is closer to convective adjustment schemes than to current mass-flux schemes because it adjusts the water column in one time step. This certainly has great consequences on the deep-water properties.

2. EDMF Parameterization

The formulation of the parameterization scheme is mainly derived from the approach developed by Soares et al. (2004) for convective cumulus parameterization in the atmosphere. The differences between the atmosphere and the ocean relate to the conservative variables and the equation of state. The oceanic conservative variables ψ considered are the potential temperature (T) and the practical salinity (S) instead of the atmospheric potential temperature, the specific humidity and the cloud water. For simplicity, "temperature" refers to "potential temperature" throughout the text in the next sections.

2.1. Mass-Flux Convection Scheme

The MF parameterization is treated as a subgrid-scale vertical process. In each horizontal model grid-cell, the convective boundary layer is composed of plumes of thermals randomly distributed. The ensemble of plumes are gathered into one single convective plume which is merged into the grid-cell environment (Figure 1). This approximation is reasonable if the plumes do not interact themselves but interact only with their environment and if the plumes properties equation is almost linear. In this manner, summation of mass fluxes over plumes converges toward the mass-flux of a single equivalent plume. The convective plume covers a fraction a_p of the grid cell, called fractional area, representing the probability of convection occurrence in a grid-cell and has conservative properties $\psi_p = (T_p, S_p)$ and a downward velocity w_p, whereas the surrounding environment has conservative properties $\psi = (T, S)$ which are the prognostic variables of the model. Under these conditions, the turbulent flux of a conservative variable ψ can be decomposed into a local diffusive flux and a nonlocal convective flux (Siebesma & Cuijpers, 1995) as follows:

$$\overline{w'\psi'} = \overline{w'\psi'}_{\text{Diffusion}} + \overline{w'\psi'}_{\text{Convection}} = \underbrace{-K_z \frac{\partial \psi}{\partial z}}_{\text{Diffusion}} \underbrace{- F_M \left(\psi - \psi_p \right)}_{\text{Convection}}, \tag{1}$$

where the mass flux is written as follows:

$$F_M = -a_p w_p. \tag{2}$$

Siebesma and Cuijpers (1995) and Wang and Stevens (2000) have shown that the mass flux contribution in Equation 1 can represent 80%–90% of the total flux of conservative variables.

The budget equation of ψ is the divergence of the diffusive and convective ψ-fluxes:

$$\frac{\partial \psi}{\partial t} = -\frac{\partial \overline{w'\psi'}}{\partial z}. \tag{3}$$

Based on the Reynolds axioms, it can be shown that the convective contribution to the total flux in Equation 3 is written as:

$$\overline{w'\psi'}_{convection} = a_p(w_p - w_e)\left(\psi_p - \psi\right) = F_M\left(\psi_p - \psi\right),$$

where w_e denotes the compensatory upward motion in a grid-cell. w_e is related to the plume and large scale vertical velocities by the mass-conservation equation in a grid-cell which writes as:

$$\overline{w} = a_p w_p + (1 - a_p)w_e,$$

where $\overline{w}$ is the resolved large scale vertical velocity which results from the continuity equation in a three-dimensional model. As shown by Suselj et al. (2019), the mass flux defined as $F_M = a_p(w_p - w_e) = \frac{a_p}{1-a_p}(w_p - \overline{w})$ is commonly approximated by $F_M = a_p w_p$ because of usually small fractional convection area ($a_p \leq 0.1$) and small resolved vertical velocity $\overline{w}$ ($\simeq 10^{-5}$ m s^{-1}) compared to the convective velocity w_p ($\simeq 10^{-2}$ m s^{-1}).

According to the Equations 1 and 2, it remains to express the plume properties $\psi_p(z)$, $w_p(z)$, and $a_p(z)$.

2.2. Plume Properties

The plume properties are represented by the variable ψ_p which includes the potential temperature (T_p) and the salinity (S_p). As in Siebesma and J.Teixeira (2000), a simple entraining rising atmospheric parcel, similar to the one used for cumulus convection (Betts, 1973), is used for the ocean:

$$\frac{\partial \psi_p}{\partial z} = -\epsilon_\psi\left(\psi_p - \psi\right), \tag{4}$$

where ϵ_ψ is the lateral entrainment rate between the plume ψ_p and the environment ψ (Figure 1). As proposed in previous atmospheric studies (Nordeng, 1994; Siebesma, 1998), ϵ_ψ has the following form:

$$\epsilon_\psi = \left|\frac{1}{w_p}\frac{\partial w_p}{\partial z}\right| + \epsilon_g. \tag{5}$$

The first component $\epsilon_o = \left|\frac{1}{w_p}\frac{\partial w_p}{\partial z}\right|$ is the organized entrainment which is controlled by the vertical velocity of the large eddies. ϵ_o is always positive or null because it is assumed that there is lateral exchanges between the plume and its environment as soon as $\frac{\partial w_p}{\partial z} \neq 0$. The term ϵ_g is the background entrainment associated with the small-scale turbulence which develops along the plume envelope.

2.3. Plume Vertical Velocity

The convective vertical velocity at any level results of the work of the buoyancy and external forces from the surface to this level. According to Gregory (2001), the stationarized vertical momentum equation is written as follows:

$$\frac{1}{2}\frac{\partial w_p^2}{\partial z} = F_b - \frac{1}{a_p\rho_p}\frac{\partial a_p\rho_p\overline{w_p'^2}}{\partial z} - \frac{1}{\rho_p}\frac{\partial \overline{p'}}{\partial z} - g\frac{\overline{p'}}{p_h}, \tag{6}$$

where $F_b = g\frac{\rho_p - \rho_e}{\rho_e}$ is the plume buoyancy acceleration, where ρ_p and ρ_e denote the potential density of the plume and the environment, respectively. Equation 6 indicates that the increase/decrease of the convective velocity in the plume results from a positive/negative work of the buoyancy force on the vertical, respectively. The plume starts as soon as $w_p > 0$ and ends at the first level where $w_p = 0$ (Figure 1). p_h is the hydrostatic pressure, and the prime denotes a perturbation around the mean hydrostatic state, and the overbar is the average over the fractional area a_p covered by plumes. The parametrization of pressure perturbation and turbulent kinetic energy transport terms in Equation 6 is still an issue for atmospheric mass-flux schemes (Léger et al., 2019) and a fortiori for ocean. Usually the turbulent kinetic energy transport term $\frac{\partial a_p\rho_p\overline{w_p'^2}}{\partial z}$ is taken as proportional to the buoyancy term F_b (Siebesma et al., 2003), while Simpson and Wiggert (1969)

approximated the effects of the pressure perturbations (third and fourth terms of Equation 6) within the plume by a drag force proportional to w_p^2. Following this idea, these pressure terms can be obtained by expressing the pressure perturbation as a function of w_p^2 as follows:

$$\overline{p'} = \alpha \rho_p w_p^2,$$

(7)

where α is a dimensionless coefficient to be defined. Throughout this study, α is kept equal to 0.2. This value was tuned to best fit the "Stratified Ocean" case presented section 3.1 because this test case has an analytical solution and was successfully reproduced by LES simulations as shown in Marshall and Schott (1999). Combining Equations 7 and 6 leads to the following plume velocity:

$$\left(\frac{1}{2} + \alpha\right) \frac{\partial w_p^2}{\partial z} = a_1 F_b - \alpha g \frac{\rho_p}{p_h} w_p^2.$$

(8)

The value of the coefficient a_1 is still a subject of research and was diagnosed close to 1 from Large Eddy Simulations (LES) studies for the atmospheric convective boundary layer (Siebesma et al., 2003). In Equation 8, the coefficient $\alpha g \frac{\rho_p}{p}$ represents the resistance applied to downward convective parcels. This resistance is inversely proportional to the pressure and thus decreases with depth.

2.4. Convective Area

The vertical profile of the fractional area a_p is deduced from the continuity equation:

$$\frac{\partial F_M(z)}{\partial z} = ent - det,$$

where *ent* and *det* are the entrainment and detrainment between the plume and the environment, respectively. The continuity equation leads to:

$$\frac{1}{a_p} \frac{\partial a_p}{\partial z} = -\mathcal{L} + \epsilon_{ap} - \delta_{ap} \quad \text{with} \quad \mathcal{L} = \frac{1}{w_p} \frac{\partial w_p}{\partial z},$$

(9)

where ϵ_{ap} and δ_{ap} are the entrainment and detrainment rates, respectively.

The shape of the vertical velocity in the convective area is such that it increases in the upper part ($\mathcal{L} > 0$) and decreases in the deeper part ($\mathcal{L} < 0$) of the plume. As consequence, the idealized situation corresponding to $\epsilon_{ap} = 0$ and $\delta_{ap} = 0$ induces a decrease/increase of a_p in the upper/lower part of the plume.

For simplicity, some authors (Nordeng, 1994; Siebesma, 1998; Soares et al., 2004) assumed that a_p remains constant. This situation is achieved if the lateral entrainment compensates exactly the narrowing of a_p in the upper part of the plume ($\epsilon_{ap} - \mathcal{L} = 0$) and if the lateral detrainment compensates exactly the broadening of a_p in the lower part of the plume ($\delta_{ap} + \mathcal{L} = 0$). As in Rio et al. (2010), we argue that the entrainment and detrainment rates lie between these two extremes, so their expressions are written as follows:

$$\begin{cases} \epsilon_{ap} = \beta_1 Max(0, \mathcal{L}) \\ \delta_{ap} = -\beta_2 Min(0, \mathcal{L}). \end{cases}$$

(10)

In this study, the coefficients β_1 and β_2 were kept equal to 0.9 that correspond to the atmospheric values (Rio et al., 2010).

2.5. Scheme Closure and Initialization

The convective closure is a problem of finding a relation between the intensity of the subgrid-scale convective activity and the large-scale variability (model-resolved variables). A wide variety of closures are proposed for the atmospheric convection to determine the mass-flux at the surface, at the top of the unstable layer or at the cloud base (Arakawa & Schubert, 1974; Rio & Hourdin, 2008).

In the oceanic parameterization presented in this paper, the scheme closure aims at defining the value of the fractional convective area at the surface a_{p0}. The closure adopted in this study is derived from Grant (2001) and Pergaud et al. (2009) because the surface buoyancy flux F_{b0} is a reliable index of the convective plumes population density and intensity.

$$F_{b0} = g \left(\gamma_1 F_{net} - \gamma_2 SSS \frac{E - P}{\rho_w} \right) l_0,$$

where $\gamma_1 = 2.10^{-4}(K^{-1})$ and $\gamma_2 = 7.10^{-5}(psu^{-1})$ are the thermal expansion and haline contraction coefficients, respectively, F_{net} ($m\ K\ s^{-1}$) is the net heat flux, SSS is the sea surface salinity, $(E-P)$ ($kg\ m^{-2}\ s^{-1})$) denotes evaporation minus precipitation, ρ_w is the surface water density, l_0 is a downward mixing length-scale kept equal to the thickness of the first layer.

After Pergaud et al. (2009), the mass-flux (F_{M0}) and the fractional convective area (a_{p0}) at the surface are linked to F_{b0} as follows:

$$\begin{cases} a_{p0} = \frac{F_{M0}}{2/3(u_* + w_*)} & \text{if } F_{M0} > 0 \text{ where } F_{M0} = C_{M0}|F_{b0}|^{1/3}sign(1, F_{b0}) \\ a_{p0} = 0 & \text{otherwise,} \end{cases} \tag{11}$$

where u_* is the surface frictional velocity and $w_* = |F_{b0}|^{1/3}$ is the surface convective velocity scale (Stull, 2003). Based on atmospheric LES results, Pergaud et al. (2009) propose $C_{M0} = -0.065$.

If the plume starts below the surface, then $a_{p0} = 0.1$.

The initial plume properties at the surface are defined as $\psi_p = \psi$ meaning that the plume starts when a static instability occurs at the surface.

2.6. Set of Equations

The system of equations which describes the Mass-Flux convection parameterization scheme is summarized as follows:

$$\begin{cases} \frac{\partial \psi_p}{\partial z} = \epsilon_\psi (\psi_p - \psi) \\ \left(\frac{1}{2} + \alpha\right) \frac{\partial w_p^2}{\partial z} = a_1 F_b(z) - \alpha g \frac{\rho_p}{\rho_h} \\ \frac{1}{a_p} \frac{\partial a_p}{\partial z} = -\frac{1}{wp} \frac{\partial w_p}{\partial z} + \epsilon_{ap} - \delta_{ap} \\ F_M = -a_p\ w_p \\ \frac{\partial \psi}{\partial t} = \frac{\partial F_M(\psi - \psi_p)}{\partial z} \\ \text{with } \epsilon_g = 0.001, a_1 = 1, \alpha = 0.2, \beta_1 = \beta_2 = 0.9, C_{M0} = -0.065. \end{cases} \tag{12}$$

Equation 3 for the tendency of ψ is discretized as the following full-implicit scheme:

$$\frac{\psi^{t+\Delta t} - \psi^{t-\Delta t}}{2\Delta t} = \underbrace{\frac{\partial}{\partial z}\left(K_z \frac{\partial \psi^{t+\Delta t}}{\partial z}\right)}_{\text{ED}} + \underbrace{\frac{\partial}{\partial z}\left(F_M^t(\psi^{t+\Delta t} - \psi_p^t)\right)}_{\text{MF}}. \tag{13}$$

The numerical unification of the ED and MF schemes into a single tridiagonal matrix represents the EDMF parameterization.

The following sections present cases of one-dimensional simulations performed with the EDMF parameterization implemented into NEMO.

The one-dimensional NEMO configuration (NEMO-1-D) is the same as that described in Reffray et al. (2015). In such configuration, there are no lateral conditions, no advections and horizontal diffusion, no horizontal divergence of currents; therefore, no vertical velocity and no horizontal pressure gradient. Only the vertical physics, the diffusion, and solar penetration parameterization schemes are activated and forced by surface momentum, heat, and water fluxes. The four cases presented in sections 3 and 4 use the same ED scheme based on the TKE parameterization.

3. Idealized Convection

This section presents an evaluation of the ability of the EDMF scheme to adjust the vertical distribution of the temperature and salinity for two academic oceanic cases which correspond to a continuously stratified ocean cooled at the surface and to a strong internal static instability of cold and dense water. For these both cases, a linear state equation is used; the salinity is fixed at $35\ psu$ and the time step (Δt) and the vertical resolution (Δz) are set at $360\ s$ and $5\ m$, respectively. In the EDMF stability tests, Δt and Δz are multiplied and divided by 5.
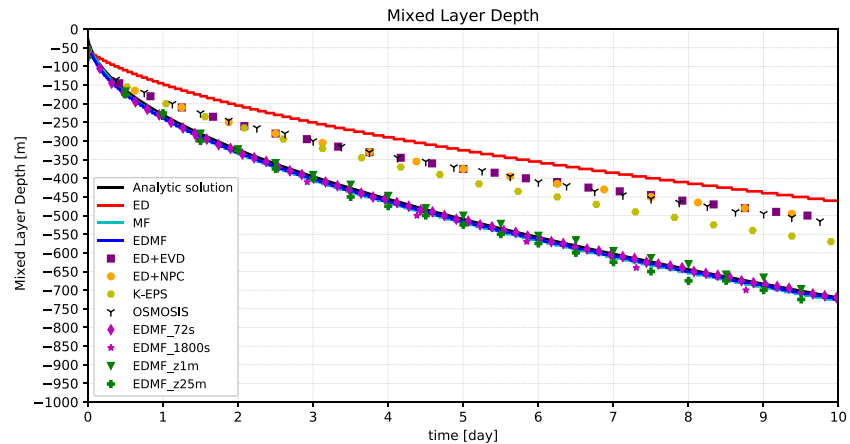
Figure 2. Mixed-layer depth evolution of a stratified ocean at rest forced by a constant surface cooling of $-500 \, \text{W m}^{-2}$. The the MLD criterion is the depth at which $(\rho(z) - \rho(z = -10)) \geq 0.01 \, \text{kg m}^{-3}$ Analytical solution (reference, black line), Eddy Diffusivity (ED = TKE, red), Eddy-Diffusivity with nonpenetrative convection (ED + NPC, orange circle), Eddy-Diffusivity with enhanced vertical diffusion (ED + EVD, $EVD = 10 \, \text{m}^2 \, \text{s}^{-1}$, purple square), $[K - \epsilon]$ scheme (light green circle), OSMOSIS scheme (black Y), Mass-Flux alone (MF, green), Eddy-Diffusivity-Mass-Flux (EDMF, blue), Eddy-Diffusivity-Mass-Flux sensitivity tests with the time step divided by 5 (72 s, purple diamond) and multiplied by 5 (1,800 s, purple star) and with the vertical discretization divided by 5 (1 m, green triangle) and multiplied by 5 (25 m, green cross).

3.1. Stratified Ocean

In this section, the erosion by convection of a resting and stratified fluid is considered to provide an idealized case for which an analytical solution can be used to validate the EDMF scheme. The case presented in Marshall and Schott (1999), which was successfully simulated by a nonhydrostatic model, is considered in this study.

In the limit that the convective layer is vertically homogeneous and as long as the stratification $N^2 = -\frac{g}{\rho}\frac{\partial \rho}{\partial z}$ (where g is the gravity and ρ the density) at the base of the mixed-layer is constant, Marshall and Schott (1999) indicate that the rate of deepening of the MLD has an analytic solution which can be derived from the following relationship:

$$\frac{\partial h}{\partial t} = \frac{\mathcal{B}}{N^2 h} \quad \text{where } \mathcal{B} \text{ is the surface buoyancy flux.} \tag{14}$$

The total water depth is 2,000 m and the initial temperature profile decreases uniformly from 3°C at the surface to 1°C at the bottom. A constant surface cooling of $-500 \, \text{W m}^{-2}$ is applied during 10 days, which corresponds to a surface buoyancy forcing $\mathcal{B} = -1. \, 10^{-7} \, \text{m}^2 \, \text{s}^{-3}$. No fresh water flux forces the surface so that the salinity profile remains constant and the Brunt-Väisälä frequency is constant equal to $N^2 = 7.65 \, 10^{-7} \, \text{s}^{-2}$ during the whole period. No surface momentum flux is applied.

Integration of Equation 14 gives the analytical evolution of the MLD during 10 days under the above idealized conditions (Figure 2). As in Marshall and Schott (1999) (see their Figure 15c), this MLD evolution is used as reference to validate and calibrate the EDMF scheme.

The vertical turbulent diffusion (ED, red line) always significantly underestimates the MLD, which is the depth at which the change in density reaches $0.01 \, \text{kg m}^{-3}$ relative to the density at 10 m depth. After 10 days, it reaches 450 m, 270 m less than the analytical solution (720 m) (Figure 2). Addition of the nonpenetrative convection (ED + NPC, orange circle) or enhanced vertical diffusion (ED + EVD, $EVD = 10 \, \text{m}^2 \, \text{s}^{-1}$, purple square) to ED and also $[K - \epsilon]$ (light green circles) and OSMOSIS (Y black) parameterizations lead to MLDs around 500 m, thus close to ED only, which are thus far from the analytical reference. These results mean that even with a strong surface buoyancy loss, these treatments of convection lack realism because of a lack of physics in their concepts. The mass-flux scheme only (MF, green line) is superimposed to the analytic solution and is much more realistic than ED, (ED + NPC), (ED + EVD), $[K - \epsilon]$ and OSMOSIS, in simulating the mixed-layer depth evolution. The differences of performances are in the differences between the convective and diffusive heat fluxes, which are discussed hereafter. EDMF (blue line) and MF (green line)
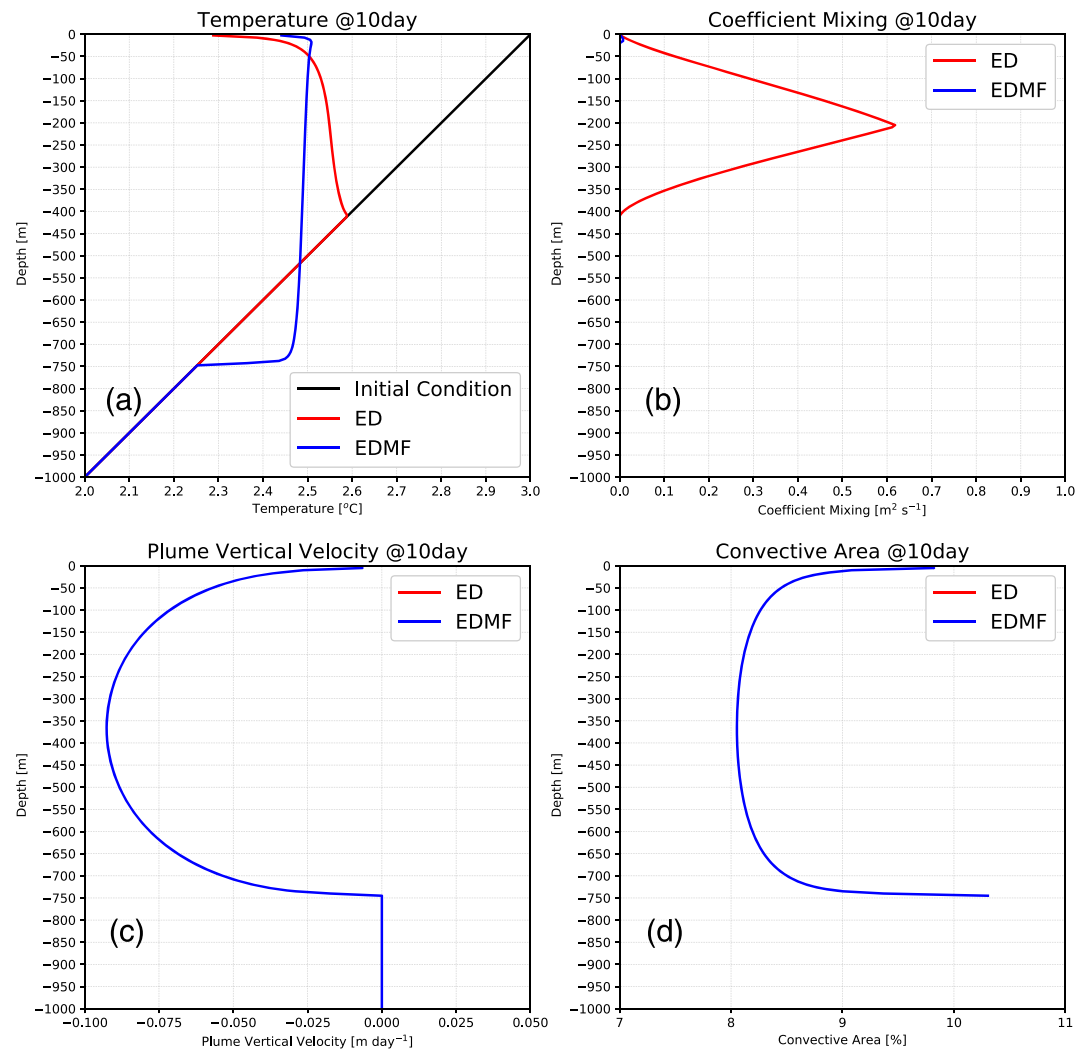
Figure 3. Vertical profiles at Day 10, i.e., the end of both ED (red) and EDMF (blue) simulations of (a) Temperature (°C), black line shows the initialization profile, (b) vertical diffusion coefficient ($m^2\,s^{-1}$), (c) convective velocity ($m\,s^{-1}$), and (d) fractional convective area (%). *Note*: No vertical velocity and convective area for ED.

are both tightly close to the analytical reference. At the end of the run, the EDMF and MF schemes simulate mixed-layer depths around 720 m that drastically improve the ED (450 m), (ED + NPC), (ED + EVD), $[K-\epsilon]$ and OSMOSIS performances (500 m) against the analytical reference (720 m) (Figure 2). The better agreements of EDMF and MF simulations with the analytical reference point out that convective processes, namely, the nonlocal vertical transports, play a fundamental role in the MLD growth.

Sensitivity tests of EDMF to the vertical resolution (Δz) and model time step (Δt) are presented in Figure 2. Δz and Δt have been multiplied and divided by 5 (25 m, 1 m, and 1,800 s, 72 s, respectively). The stability of the solutions to variations of Δz and Δt is noteworthy and shows the consistency of the EDMF numerical scheme.

Profiles of temperature simulated by ED and EDMF at the end of the run (Figure 3a) display MLDs bounded and unbounded by the stratified region, respectively. The overshooting obtained with EDMF means an intrusion of warm and light water into the stratified zone between -500 and -720 m. In order to go further into the analysis of these differences, the vertical diffusion coefficient (K_z) and the convective velocity (w_p) are inspected (Figures 3b and 3c). With the ED scheme, coefficient K_z controls the vertical mixing as long as the temperature profile is unstable ($\frac{\partial T}{\partial z} < 0$) and stops as soon as the stratification is stable ($\frac{\partial T}{\partial z} > 0$) because the buoyancy source of TKE vanishes.

When EDMF is active, the energy of buoyancy is distributed between diffusion and convection, but in this case, this energy is almost fully used to supply convection and not diffusion. Indeed K_z is very weak and trapped in the first levels close to the surface (Figure 3b). The vertical mixing is fully controlled by the donwnward convective velocity (Figure 3c) which increases and reaches its maximum close to $w_{max} = -10\,\mathrm{cm\,s^{-1}}$ around $-400\,\mathrm{m}$ depth. Below this level, the convective parcels enter the stable part of the mixed-layer and reach their level of no motion around $-750\,\mathrm{m}$ depth.

The convective fractional area varies vertically according to the mass conservation equation (see Equation 9), as a consequence, it decreases/increases in the upper/lower layers where the convective velocity intensity increases/decreases (Figure 3d). A sharp increase of this area occurs at the mixed-layer base resembling an anvil of cumulonimbus in the atmosphere. This behavior is an important ingredient to generate an overshoot or penetrative convection as shown in Figure 3a.

The total heat flux (FT) can be split into its diffusive (FD) and convective (FC) parts as:

$$\begin{cases} FT = FD + FC \\ FD = \overline{w'T'} = K_z \frac{\partial T}{\partial z} \\ FC = F_M(T - T_p). \end{cases} \tag{15}$$

FD and FC are analyzed when diffusion only is active (ED) and when EDMF (ED coupled with MF) is active. For ED and EDMF, diffusive fluxes are FD_ED and FD_EDMF, respectively, and convective fluxes are FC_ED and FC_EDMF, respectively. Note that there is no convection for ED then $FC\_ED = 0$. In such conditions $FT\_ED = FD\_ED$ and $FT\_EDMF = FD\_EDMF + FC\_EDMF$.

FC_EDMF is negative (downward) in upper layers and becomes positive (upward) in the lower part of the mixed-layer (Figure 4b). This lower part corresponds to the stratified zone in which the mass-flux F_M slows down and finally vanishes at $z = -750\,\mathrm{m}$ (Figure 4a). The penetration of the convective plumes into the stratified area characterizes the overshoot and plays a crucial role in the entrainment process at the mixed-layer base as shown by the strong intensities of FC_EDMF ($\simeq 7\,\mathrm{K\,m\,day^{-1}}$).

FD behaves differently with and without convection. In case of pure diffusion ($FT\_ED = FD\_ED$, no convection), FD_ED is negative and close to FC_EDMF in upper-layers (0, $-400\,\mathrm{m}$). With convection, FD_EDMF strongly weakens compared to FD_ED and is limited to the first 15 m below the surface meaning that convection consumes a large part of the available buoyancy energy to the detriment of diffusion in this layer. FD_ED vanishes around $z = -400\,\mathrm{m}$ at the beginning of the stratified layer ($\frac{\partial T}{\partial z} > 0$) precisely where FC_EDMF changes sign. This sign change means that the convective heat flux is counter-gradient, namely, opposite to the local temperature gradient. This result is obtained thanks to the work of the buoyancy forces which give rise to a nonlocal convective velocity.

3.2. Static Instability

In this section, we evaluate the ability of the EDMF parameterization at simulating the convection at any level and not only in the mixed-layer. In addition the internal static instability case considered is intentionally unrealistic in order to highlight the robustness of the EDMF numerical scheme.

In a one-dimensional approach, the static instability profile (Figure 5, black line) is represented by a 50 m thick slab of cold water 50 m below the surface. The strong initial instability of 5°C overhangs a stable layer which starts at $-200\,\mathrm{m}$ depth down to the bottom. No heat and momentum fluxes force the surface during the 1 day simulation.

The diffusion (ED) and convection (MF) components of EDMF are switched on and off to quantify the effects of diffusion and convection separately and both together (EDMF) on the prognostic variables and also to test the robustness of the numerical scheme under extreme conditions.

After 1 day, the simulated temperatures reach their equilibrium (Figure 5). The ED scheme (red profile) mixes the temperature from the first unstable level at $z = -50\,\mathrm{m}$ down to the limit of the stratified layer at $z \simeq -310\,\mathrm{m}$ depth. Four other simulations were performed. Two by coupling the nonpenetrative convection (NPC) and the enhanced vertical diffusion ($EVD = 10\,\mathrm{m^2\,s^{-1}}$) with the ED scheme and two others with the $[K - \epsilon]$ and OSMOSIS parameterizations. Experiments ED + NPC (orange circle), ED + EVD (purple square), $[K - \epsilon]$ (light green circle) and OSMOSIS (black Y) simulate vertical profiles very close to ED. Note
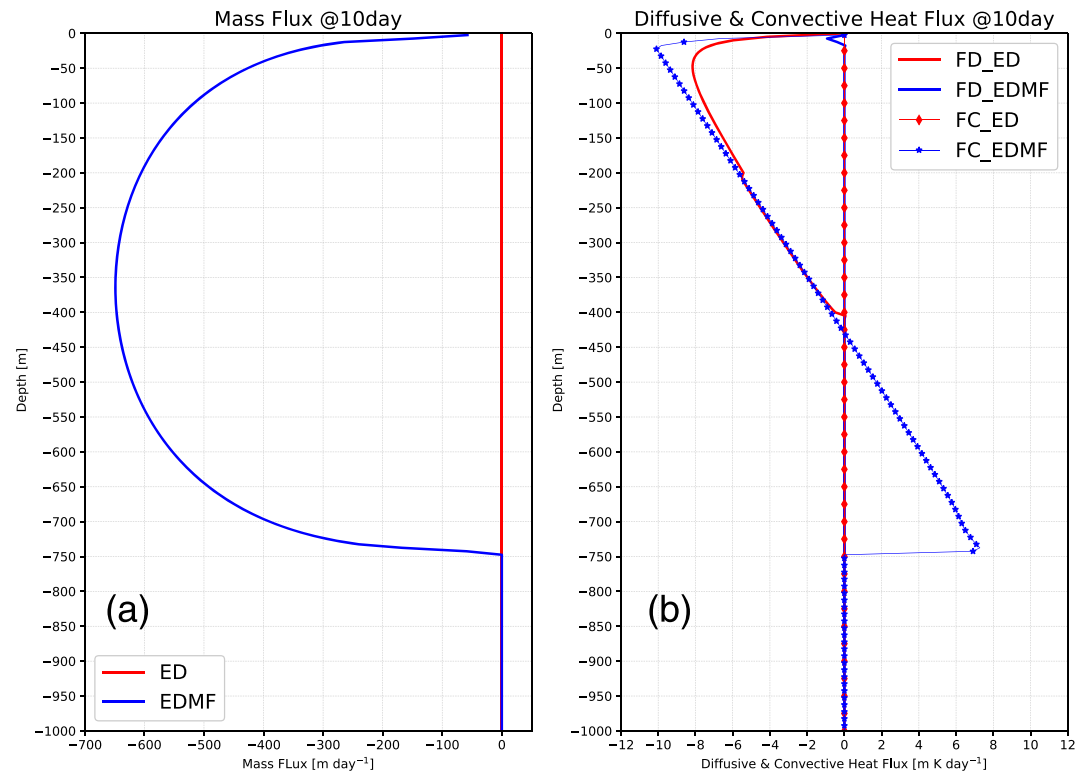
Figure 4. Vertical profiles at the end of both ED and EDMF simulations of (a) Mass Flux (F_M, m day^{-1}), (b) Diffusive fluxes (m K day^{-1}) for Eddy-Diffusivity alone (FD_ED, red solid line) and Eddy-Diffusivity-Mass-Flux (FD_EDMF, blue solid line). Convective fluxes (m K day^{-1}) for Eddy-Diffusivity alone (FC_ED, red dashed line) and Eddy-Diffusivity-Mass-Flux (FC_EDMF, blue dashed line) (FC_ED, red bullet line) and Eddy-Diffusivity-Mass-Flux (FC_EDMF, blue star line).

also that ED + NPC, ED + EVD, $[K - \epsilon]$ and OSMOSIS better stabilize the temperature profile than ED and $[K - \epsilon]$ mixes upwards to the surface due to bi-directional mixing-lengths.

MF scheme mixes the temperature down to inside of the stratified layer ($z \simeq -600$ m) while all ED schemes stop at -310 m . The penetrative convection driven by the vertical velocity w_p is thus more efficient in destroying the stratified layer than the diffusion. EDMF scheme simulates a state close to MF meaning that the buoyant energy is mainly used to supply convection than diffusion in this case.

As in section 3.1, sensitivity tests of EDMF solutions to the same variations of Δz and Δt were conducted in this case and presented in Figure 5. The stability of the solutions confirms the consistency of the numerical scheme that gives confidence in the results.

The static instability and stratified ocean cases have shown that the numerical scheme of EDMF is consistent and robust and is able to reproduce the LES simulations of convection under strong surface buoyancy loss presented in Marshall and Schott (1999).

4. Real-Ocean Cases

The performance of the EDMF parameterization is now evaluated with two real one-dimensional situations. The first one corresponds to sequences of strong convective events which were documented in the Northwestern Mediterranean during winter 2013 of the HyMeX/ASICS-MED experiment (Estournel et al., 2016) at the LION buoy. The second one corresponds to weak and moderate mixing events which occurred at the PAPA station located in the North Pacific Ocean. This buoy is located in a region of weak horizontal advection and is commonly used by the community to validate turbulent closures (Burchard, 2001; Reffray et al., 2015).
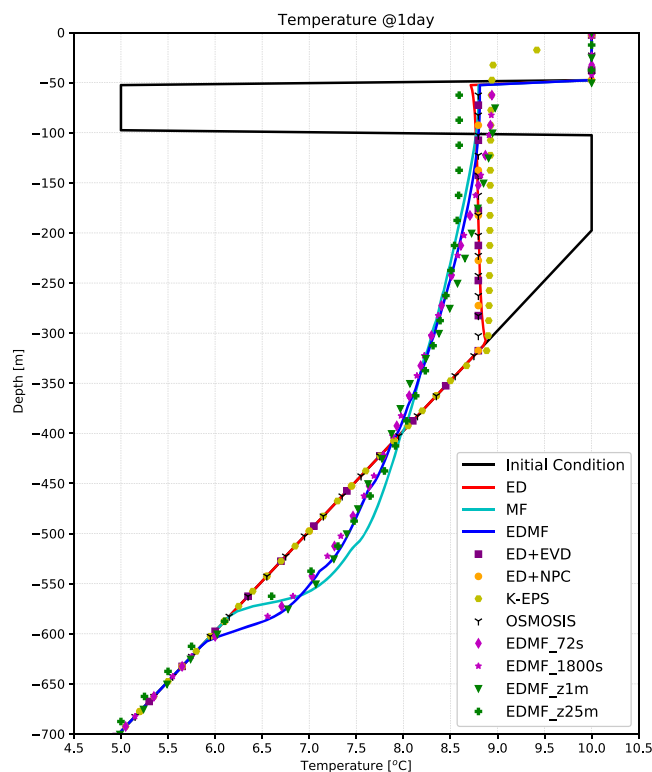
Figure 5. Initial temperature (°C, black). One day simulated temperature with vertical eddy diffusivity scheme alone (ED, red), Eddy-Diffusivity with nonpenetrative convection (ED + NPC, orange circle), Eddy-Diffusivity with enhanced vertical diffusion (ED + EVD, $EVD = 10\,\mathrm{m^2\,s^{-1}}$, purple square), $[K - \epsilon]$ scheme (light green circle), OSMOSIS scheme (black Y), Mass-Flux alone (MF, green), Eddy-Diffusivity-Mass-Flux (EDMF, blue), Eddy-Diffusivity-Mass-Flux sensitivity tests with the time step divided by 5 (72 s, purple diamond) and multiplied by 5 (1,800 s, purple star) and with the vertical discretization divided by 5 (1 m, green triangle) and multiplied by 5 (25 m, green cross).

Both cases presented in this section use the EOS80 (UNESCO, 1981) equation of state, a time step $\Delta t = 360\,\mathrm{s}$ and a vertical grid of 75 levels with a first level at 1 m below the surface and 24 levels in the first hundred meters. This vertical grid was used by Reffray et al. (2015) in their one-dimensional study of vertical diffusion parameterizations and currently used in the NEMO community as for instance to produce the CMEMS reanalyses (ECMWF, MetOffice, CMCC and Mercator) (Storto et al., 2019). The initial conditions were provided by the in situ T/S data collected at the LION and PAPA buoys and interpolated on the model vertical grid.

4.1. The Northwestern Mediterranean

Convection in the Gulf of Lion is induced by high levels of cooling and evaporation due to the prevailing cold, dry, northerly local winds (Mistral and Tramontane), along with cyclonic circulation associated with the doming of isopycnals, which facilitates mixing with the saltier underlying waters. During winter, the cyclonic circulation is reinforced, isolating water in the gulf's central part and favoring heat loss. Convection in the Gulf of Lion exhibits interannual variability, both in time (years with or without dense water formation) and in space. The vertical extent of the convection varies between a few hundred meters and the whole water column (~2,500 m Mertens & Schott, 1998; Somot et al., 2016), and its horizontal extent from a few tens of kilometers to ~100 km. This convection feeds thermohaline circulation through the transformation of waters of Atlantic origin into intermediate and deep water masses, called Winter Intermediate Water and Western Mediterranean Deep Water, respectively.

The ASICS-MED experiment, which was the oceanographic component of the HYdrological cycle in the Mediterranean Experiment (HyMeX, 2010-2020 Drobinski et al., 2014), aimed at monitoring the thermohaline characteristics of the water masses in the Gulf of Lion during winter 2012 and 2013 at high frequency. The enhanced monitoring network (autonomous profiling floats and gliders as well as dedicated research cruises, Estournel et al., 2016) targeted the most interesting events in order to document the oceanic mixed layer deepening through convection and the processes of dense water formation (Lebeaupin et al., 2014; Léger et al., 2016; Giordani et al., 2017).

The Météo-France meteorological buoy MF-LION, located at 42.07°N, 4.66°E provides atmospheric observations of surface pressure, wind, air temperature, humidity, radiative fluxes, and sea surface temperature and salinity. The atmospheric parameters and the oceanic data collected during the HyMeX experiment were used to compute heat, water, and momentum fluxes which close the mixed-layer heat and water budgets at the scale of the northwestern Mediterranean basin (Caniaux et al., 2017).

The LION mooring (Testor et al., 2018) is located in the center of the convection zone at 42.04°N, 4.69°E (i.e., 4–4.5 km from the MF-LION buoy location) where the seabed is found at a depth of 2,300 m. The mooring position is about where the center of the deep convection area is supposed to occur (Leaman & Schott, 1991; MEDOC-Group, 1970; THETIS-Group, 1994). The evolution of the instrumented line and details about the instruments and the calibration are given in Houpert et al. (2016).

The LION mooring is thus optimally located for evaluating the capability of the EDMF parameterization scheme to capture the evolution of hydrology during winter 2013 in the Gulf of Lion.

Measurements of temperature and salinity have been taken between 9 January and 26 March, but due to a strong horizontal advection event on 11 January (not shown in the paper), we have decided fixing the study period from 15 January to 26 March. The time series of temperature and salinity measured at the buoy mooring are presented on Figures 6a and 6b. The warm and salty waters located around 400 m depth up to 23 January correspond to the presence of the Levantine intermediate waters (LIW; Estournel et al., 2016).
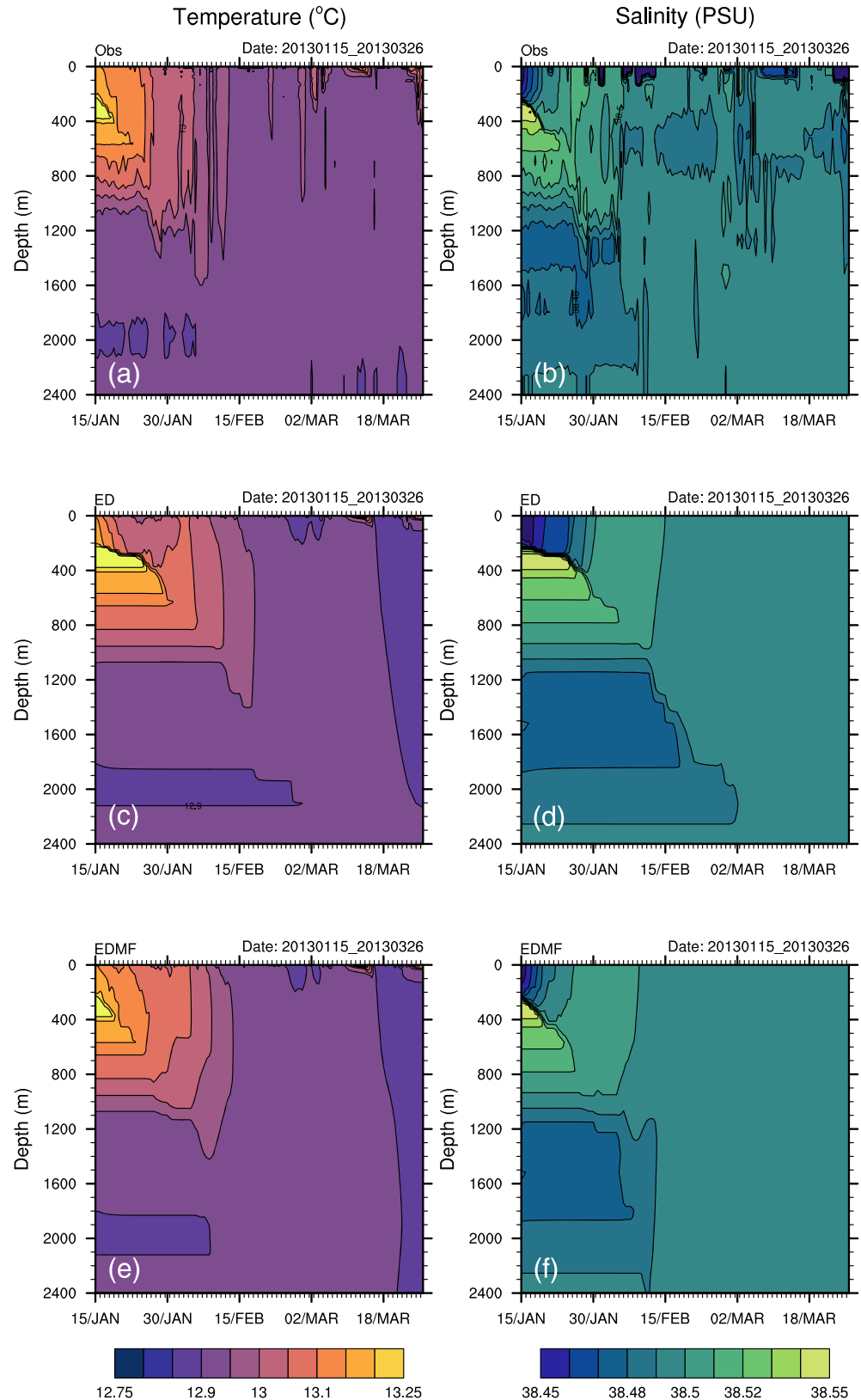
Figure 6. Time series at the Lion buoy of temperature (°C, left) and salinity (*psu*, right) for (a,b) observation, (c,d) ED scheme, and (e,f) EDMF scheme.

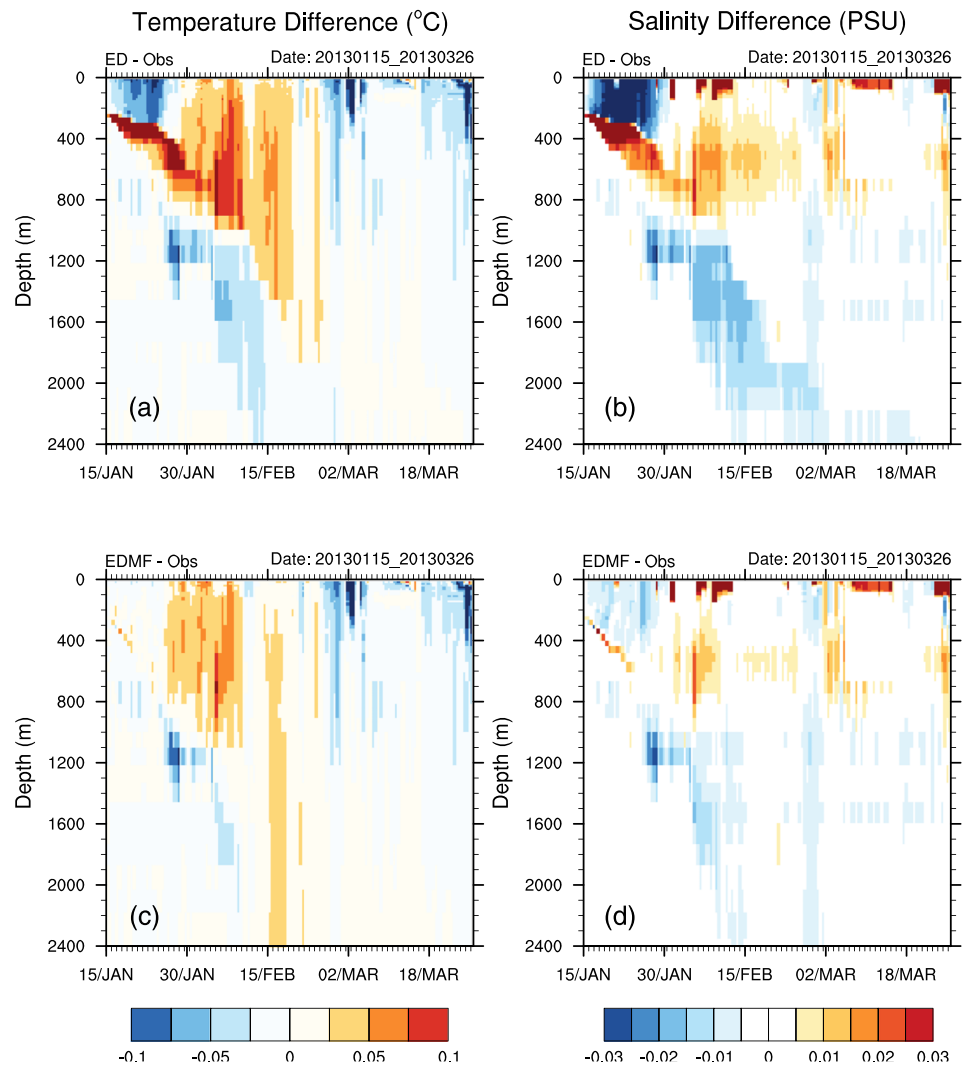**Figure 7.** Time series at the Lion buoy of temperature biases (°C, left) and salinity biases (*psu*, right) for (a,b) ED scheme and (c,d) EDMF scheme.

Erosion of LIW is caused by the vertical mixing controlled by the surface buoyancy heat loss. By destroying LIW, the vertical mixing tends to warm up and salinize the mixed-layer. When LIWs disappear from 23 January, the mixed-layer cools down and refreshes under the effect of surface fluxes. On 9 February, the water column is well mixed down to the bottom that corresponds to the first date at which the convection reached the bottom as observed by Argo floats (Coppola et al., 2017).

The initial conditions of the model were provided by the observed profiles of temperature and salinity on 15 January. Heat, water, and momentum fluxes of Caniaux et al. (2017) were used as surface forcing. Temperature and salinity simulations performed with ED (Figures 6c and 6d) display the presence of LIWs over a too long period of time, a too strong stratification and a too cold mixed-layer in comparison with observations (Figures 6a and 6b). The simulation performed with the EDMF scheme leads to temperature and salinity (Figures 6e and 6f) in better agreement with observations, particularly in terms of timing of LIW destruction and of first occurence of a mixed-layer (T and S) down to the sea floor on 9 February (Coppola et al., 2017). Scores of temperature and salinity obtained with the ED and EDMF schemes (Figure 7) show significant reduction of biases with EDMF mainly during the deepening period, namely, up to 14 February. After this date, the water column is well mixed, and the following convective events do not change significantly the water properties anymore. During the deepening phase, EDMF decreases the temperature and salinity biases in the thermocline and in the mixed-layer against the ED scheme because the convection readjusts the thermocline stratification more realistically.

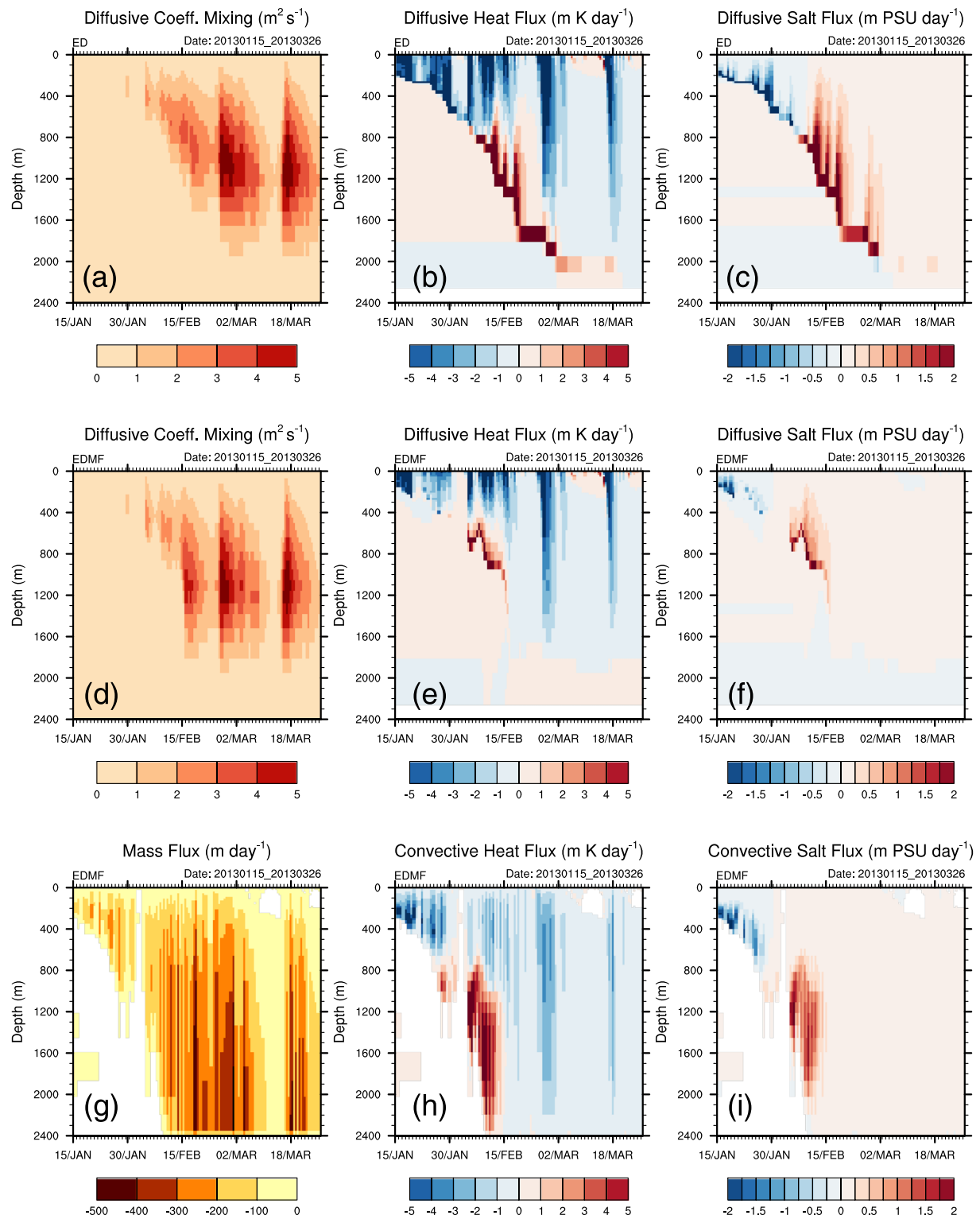**Figure 8.** Time series at the Lion buoy of (a,d) the vertical coefficient mixing (m² s⁻¹), (g) the mass-flux (m day⁻¹), (b,e,h) the vertical heat flux (m K day⁻¹) and (c,f,i) the vertical haline flux (m psu day⁻¹) for the ED alone (top), ED in EDMF (middle) and Mass-Flux in EDMF (bottom) schemes.

Coupling convection with diffusion in EDMF impacts the coefficient of vertical mixing (K_z). As shown in Figures 8a and 8d, convection tends to decrease the magnitude of K_z because part of the available buoyancy energy is used for convection. With respect to the ED scheme, EDMF induces a weakening of diffusive fluxes of temperature (Figures 8b and 8e) and salinity (Figures 8c and 8f), particularly during the strongest deepening phase between the 9 and 14 of February. Such differences reflect the part of the buoyancy energy used by the convection which is no more available to produce TKE. The convective available potential energy (CAPE) which results of the work of the buoyancy force on the vertical is used to produce the convective velocity and then the mass-flux (F_M) in plumes (Figure 8g). The time series of F_M (Figure 8g) shows the intermittency of the convection activity which is tightly connected with surface buoyancy loss (not shown). The strongest buoyancy loss events associated with strong northerly winds induce mass-flux up to $-500\,\mathrm{m\,day^{-1}}$. Note that convective plumes first reach the bottom on 9 February in accordance with observations. After a stratification period, during which surface buoyancy fluxes are positive, a new wind gale occurred on 15 March which induced surface buoyancy loss around $-800\,\mathrm{W\,m^{-2}}$ and convective mass-flux again up to $-500\,\mathrm{m\,day^{-1}}$ over the whole water column (Figure 8g). This was the last convective event of the year. During the deepening phase up to 9 February, the associated convective heat and haline fluxes (Figures 8h and 8i) display stronger intensities in the entrainment zone, namely, in the thermocline, than diffusion heat and haline fluxes shown Figures 8e and 8f, respectively. Stronger convective fluxes than diffusion fluxes point out the greater capability of the convective velocity to penetrate into the stratified entrainment zone than turbulence. Note that after 9 February, diffusion fluxes are more active than convection fluxes especially in upper-layers.

4.2. The Northeastern Pacific

Aim of this section is to investigate the behavior of EDMF in a region of weak to moderate vertical mixing where the vertical diffusion produced excellent results (Reffray et al., 2015).

The PAPA station, located west of Canada, in the Pacific Ocean (50°N, 145°W) was chosen because it is not a spot of deep or intermediate convection and has been extensively studied in the literature (Burchard, 2001; Gaspar et al., 1990; Mellor & Durbin, 1975; Reffray et al., 2015). The resulting measurements are particularly well suited for a study following a 1-D approach, and for validating and calibrating any turbulence model. Indeed, there is no interaction with the coast and the horizontal advections of heat and salt are weak. High-quality measurements of ocean properties (temperature, salinity, velocities) are available for this site (http://www.pmel.noaa.gov/OCS/Papa/).

In this section, the ED and EDMF parameterizations are evaluated with respect to the temperature and salinity collected at the PAPA station between 15 June 2010 and 15 June 2011 (Figures 9a and 9b), according to the same NEMO-1-D configuration presented in Reffray et al. (2015). The observed profiles of temperature and salinity on 15 June 2010 are the initial conditions of the model, and the surface fluxes were provided by operational ECMWF.

The warming occurs during summer time and propagates down to $-40\,\mathrm{m}$ depth by mid-September. After mid-September, the cooling starts and the thermocline deepens down to $-80\,\mathrm{m}$ by early December. From early March, the temperature decreases and is well-mixed down to $-120\,\mathrm{m}$ depth. A weak seasonal halocline (32.7 psu) visible during fall (SON) is colocated with the thermocline while a permanent and strong halocline is present around $-80\,\mathrm{m}$ depth (Figure 9b).

The ED scheme fairly well reproduces the observed temperature evolution (Figures 9a and 9c). However between July and October the simulated warming (Figure 9c) is weaker and shallower than in observations (Figure 9a). Also the cooling from early March occurs over shallower layer in simulation than in observations and ED captures the observed seasonal halocline (Figures 9b and 9d).

From July to December, EDMF (Figure 9e) deepens the thermocline more than ED alone (Figure 9c) but in excess in comparison with observations (Figure 9a). However, the cooling early March is now well captured. The mixed-layer around $-120\,\mathrm{m}$ depth obtained with EDMF against $-80\,\mathrm{m}$ obtained with ED is due to activation of convective plumes which start from the surface and reach $-100\,\mathrm{m\,day^{-1}}$ (Figure 10). These plumes penetrate continuously deeper between early September and March and control the deepening rate of the mixed-layer as shown on Figure 9e. In March, the convective plumes exceed $-120\,\mathrm{m}$ depth and collapse mid-April to occur only close to the surface in response to the restratification regime. EDMF also captures the observed weak seasonal halocline evolution (Figures 9b and 9f). Consistent with the observations
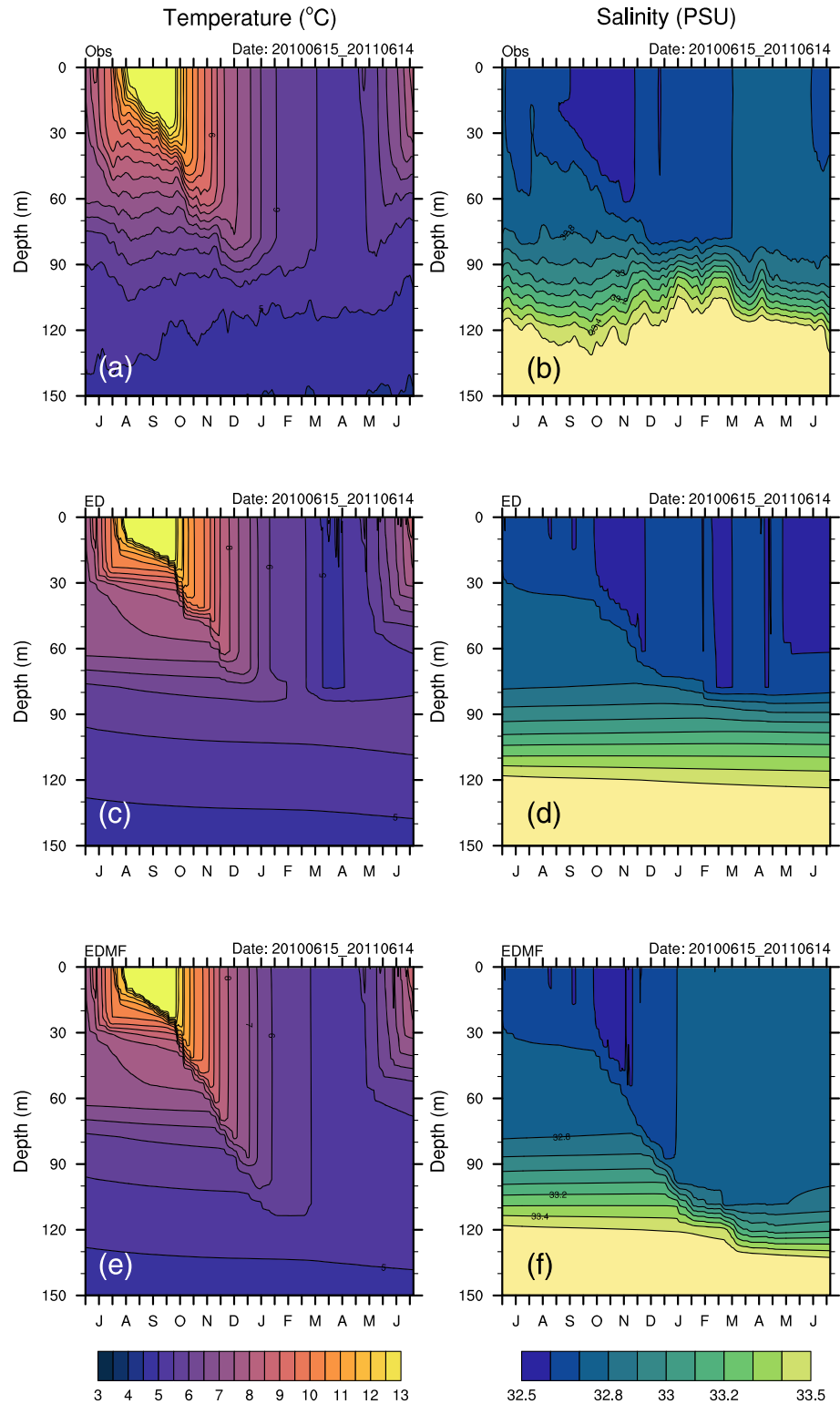
Figure 9. Time series at the PAPA station of the temperature (°C, left) and salinity (*psu*, right) for the (a,b) observations (c,d) ED and (e,f) EDMF schemes.
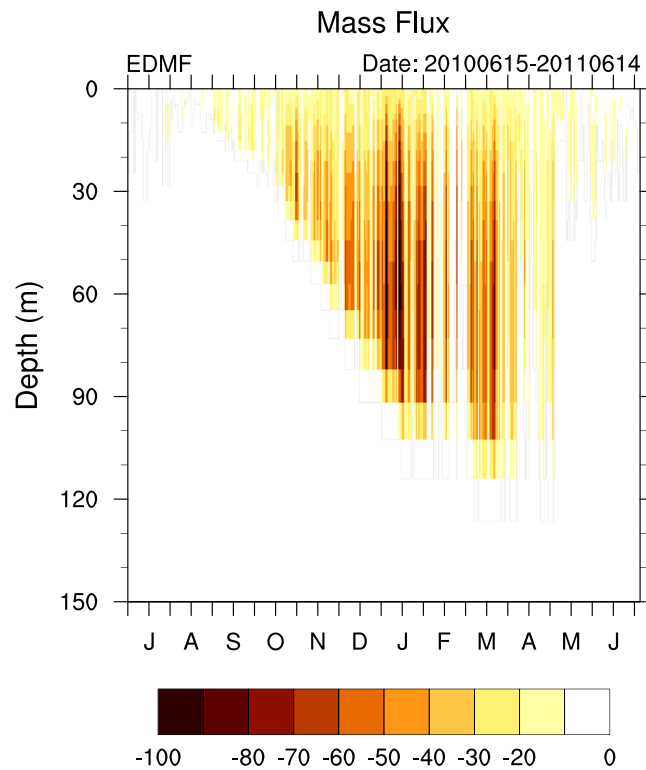
Figure 10. Time series at the PAPA station for the EDMF scheme of the vertical masss flux (m day^{-1}).

(Figure 9b), ED does not impact the permanent halocline around -80 m depth while EDMF deepens it because of too strong convective plumes (Figure 10).

The performances of ED and EDMF schemes are demonstrated only in terms of the depth-time evolution of temperature (Figures 11a and 11b) because similar conclusions were obtained with the salinity. Before end of September, biases of the ED and EDMF schemes are similar because no convective activity occurs. During the deepening phase, which starts late September, ED displays positive/negative biases inside/outside the mixed-layer (Figure 11a). EDMF reduces these biases compared to ED up to November thereafter positive biases occur in the thermocline because of strong downward heat convective transport (Figure 11b). For the same reasons negative biases of salinity were obtained in the permanent halocline (not shown).
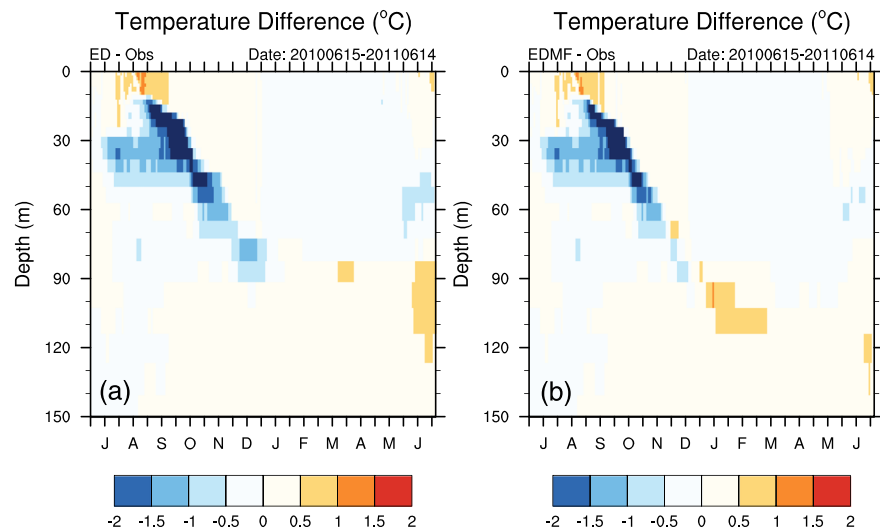

Figure 11. Time series at the PAPA station of temperature biases (°C) for (a) ED scheme and (b) EDMF scheme.

These results suggest that the convective transport of tracers is too strong for weak vertical mixing regimes, but for such regimes, EDMF has the same degree of realism as ED. However, it is noteworthy that isotherm 5°C raises 50 m in 1 year in observations (Figure 11a). This strongly suggests the presence of an advection which cannot be simulated with a one-dimensional approach. With this advection, the convective transport simulated by EDMF would be probably weaker because of stronger negative CAPE.

5. Conclusions

This study proposes a unification of eddy diffusivity and mass flux processes into an Eddy-Diffusivity-Mass-Flux (EDMF) parameterization to represent simultaneously the turbulent and convective transports in the ocean. This approach, which is broadly used in atmospheric models nowadays, has the conceptual advantage that the boundary layer is described by a single scheme that has local (diffusive) and nonlocal (mass-flux) turbulence closures. No switching to a separate convection scheme is then necessary.

The EDMF parameterization is evaluated in one-dimensional two academic and two real cases. The Marshall and Schott (1999) academic case has shown the inability of the ED scheme alone to capture the analytic evolution of a constant stratified layer forced by a surface buoyancy loss of $-500 \, \text{W m}^{-2}$ during 10 days. This failure was drastically reduced with EDMF because the mass-flux scheme generates convective vertical velocities and heat fluxes particularly active in the lower and stratified part of the mixed-layer, precisely where the turbulence vanishes. The academic case of extreme static instability (never found in nature) inside the ocean allowed to evaluate the convective scheme alone, namely with the turbulence scheme off. This evaluation has shown the robustness of the numerical implementation in the NEMO code, the heat-content conservation and the ability of the scheme to generate penetrative convection and therefore counter-gradient fluxes in stratified zones (thermocline overshooting). Practically, the EDMF parameterization aims at replacing the counter-gradient flux term introduced in ED parameterizations (Large et al., 1994; Large, 1998; Mailhôt & Benoit, 1982), the nonpenetrative convection and the enhanced vertical diffusion parameterizations.

The Northwestern Mediterranean real case was an opportunity to evaluate the EDMF parameterization during winter 2013 thanks to the HyMeX/ASICS experiment which provided in situ data and surface heat, water, and momentum fluxes in accordance with the mixed-layer heat and water budgets (Caniaux et al., 2017). This aspect is particularly important because simulation biases are often due to large uncertainties on surface fluxes. The performance of the EDMF scheme has shown promising results. The evolutions of the mixed-layer temperature and salinity during the deepening phase, the dissipation time of the Levantine intermediate water, the first occurrence of convection at sea floor on 9 February and the last strong convective event on 15 March are all well captured.

The Northeastern Pacific real case confirmed the realism of the EDMF parameterization for weak vertical mixing regimes. This is an important point because the enhanced vertical diffusion commonly used in OGCMs can generate spurious behaviors, as in equatorial regions, for instance. However, this case pointed out a deterioration of the scores with EDMF in comparison with ED scheme because of too strong vertical convective transports and probably biased ECMWF surface fluxes. Note that in the academic and Mediterranean cases the surface fluxes were controlled.

Coupling the proposed mass-flux scheme to various second-order turbulence closures parameterizations ($[k - kl]$, Mellor & Yamada, 1982; $[k - \epsilon]$, Rodi, 1987; $[k - \omega]$, Wilcox, 1988; generic lengh scale, Umlauf & Burchard, 2003) is a perspective to investigate the route taken by the buoyancy energy between diffusion and convection, which is still an open issue. While the EDMF scheme leads to realistic temperature and salinity profiles, large uncertainties remain on the lateral entrainment and detrainment rates which control the exchanges of water between the plumes and the environment and thus the buoyancy and vertical velocity in the plumes. Their evaluation in atmospheric mass-flux parametrizations generally rely on large-eddy simulations, whose resolution is fine enough to explicitly account for coherent structures within convective boundary layers (Brown et al., 2002; Couvreux et al., 2005; Moeng & Wyngaard, 1988; Siebesma et al., 2003). A similar methodology is planed for the present oceanic mass-flux parametrization. As the momentum and TKE balances were not modified in the EMDF scheme, it is suggested that nonlocal transports should also be added to those equations. Ice formation introduces a salt flux due to haline rejection that forces the convection at the surface. The impact of this salt flux will be studied in EDMF under ice growth conditions. The

surface buoyancy loss is the main driver of convection velocity but surface wind-stress induced vertical velocity could be also added to initiate vertical transport (D'Asaro, 2001), which could have significant impacts on mixed-layer tracers in stratified regimes. This question will have to be investigated in combination with the waves effects on the surface wind-stress.

Our next step is to investigate the impact of the EDMF implementation in global simulations with the full 3-D NEMO model. We will in particular investigate the impact on the hydrological properties of the water masses in regions that are prone to convection such as the Labrador and Irminger Seas, on the thermohaline overturning circulations as well as on the diurnal cycle of the mixed-layer temperature and SST at global scale. We will also evaluate the effects of the convection velocities on the biogeochemical properties of water masses. Floats observations have shown that the convective vertical velocities reach roughly 1,000 m per day during wintertime in the north Atlantic (Steffen & D'Asaro, 2002). These velocities mix the biogeochemical materials over the convective layer and are able to get back into the euphotic zone those that have sunk to depth. As mentioned by D'Asaro (2008), these convective cells could provide a seed population for the spring bloom.

Data Availability Statement

All simulations presented in this paper are based on NEMO_relase_4.0.1 (revision: 12299) and supplementary routines and input data dedicated to configurations and convection are available on Mercator Ocean International ftp (*ftp://ftp.mercator-ocean.fr/download/users/rbourdal/CONVECTION/ EXPERIMENTS/CONVECTION_EXPERIMENTS.tar*).

References

Aagaard, K., & Carmack, E. C. (1989). The role of sea ice and other fresh water in the arctic circulation. *Journal of Geophysical Research*, *94*, 14,485–14,498.

Arakawa, A., & Schubert, W. H. (1974). Interaction of a cumulus cloud ensemble with the large-scale environment. part i. *Journal of the Atmospheric Sciences*, *31*, 674–701.

Betts, A. (1973). Non-precipitating convection and its parameterization. *Quarterly Journal of the Royal Meteorological Society*, *99*, 178–196.

Brown, A., R, R. C., Cederwall, R. T., Chlond, A., Duynkerke, P. G., Golaz, J.-C., Khairoutdinov, M., et al. (2002). Large-eddy simulation of the diurnal cycle of shallow cumulus convection over land. *Quarterly Journal of the Royal Meteorological Society*, *128*, 1075–1093.

Burchard, H. (2001). On the q2l equation by mellor and yamada (1982). *Journal of Physical Oceanography*, *31*, 1377–1387.

Caniaux, G., Prieur, L., & Giordani, H. (2017). An inverse method to derive surface fluxes from the closure of oceanic heat and water budgets: Application to the North-western Mediterranean Sea. *Journal of Geophysical Research: Oceans*, *122*, 2884–2908. https://doi.org/10.1002/2016JC012167

Capet, X., Williams, J. M., Molemaker, M., & Shchepetkin, A. (2008). Mesoscale to submesoscale transition in the California Current System. Part II: Frontal processes. *Journal of Physical Oceanography*, *38*, 44–64.

Clarke, R. A., & Gascard, J. C. (1983). The formation of Labrador Sea water: Large scale processes. *Journal of Physical Oceanography*, *13*, 1764–1778.

Coppola, L., Prieur, L., Taupier-Letage, I., Estournel, C., Testor, P., Lefèvre, D., et al. (2017). Observation of oxygen ventilation into deep waters through targeted deployment of multiple Argo-O2 floats in the north-western Mediterranean Sea in 2013. *Journal of Geophysical Research: Oceans*, *122*, 6325–6341. https://doi.org/10.1002/2016JC012594

Couvelard, X., Lemarié, F., Samson, G., Redelsperger, J.-L., Ardhuin, F., Benshilad, R., & Madec, G. (2019). Development of a 2-way coupled ocean-wave model: Assessment on a global NEMO(v3.6)-WW3(v6.02)coupled configuration. *Geoscientific Model Development*, 1–36. https://doi.org/10.5194/gmd-2019-18

Couvreux, F., Guichard, F., Redelsperger, J.-L., Flamant, C., Masson, V., Kiemle, C., & Lafore, J.-P. (2005). Water vapour variability within a convective boundary layer assessed by large eddy simulations and IHOP observations. *Quarterly Journal of the Royal Meteorological Society*, *131*, 2665–2693.

D'Asaro, E. A. (2001). Turbulent vertical kinetic energy in the ocean mixed layer. *Journal of Physical Oceanography*, *31*, 3530–3537. https://doi.org/10.1175/1520-0485(2002)031<3530:TVKEIT>2.0.CO;2

D'Asaro, E. (2008). Convection an d the seeding of the North Atlantic bloom. *JMS*, *69*(3-4), 233–237.

Deardorff, J. W. (1966). The Counter-Gradient Heat Flux in the Lower Atmosphere and in the Laboratory. *Journal of the Atmospheric Sciences*, *23*, 503–506.

Drobinski, P., Ducrocq, V., Alpert, P., Anagnostou, E., Béranger, K., Borga, M., et al. (2014). HyMeX, a 10-year multidisciplinary program on the Mediterranean water cycle. *Bulletin of the American Meteorological Society*, *95*, 1063–1082. https://doi.org/10.1175/BAMS-D-12-00242.1

Ertel, H. (1942). Der vertikale Turbulenz-Wärmestrom in der Atmosphäre. *Meteor Z*, *59*, 1690–1698.

Estournel, C., Beguery, L., Belamari, S., Béranger, K., Beuvier, J., Bouin, M.-N., et al. (2016). HyMeX-SOP2, the field campaign dedicated to dense water formation in the northwestern mediterranean. *Oceanography*, *29*(4), 196–206. https://doi.org/10.5670/oceanog.2016.94

Fritsch, J. M., & Chappell, C. F. (1980). Numerical prediction of convectively driven mesoscale pressure systems. 1. Convection parameterization. *Journal of the Atmospheric Sciences*, *37*, 1722–1733.

Gascard, J. C. (1991). Open ocean convection and deep water formation revisited in the mediterranean, labrador and weddell seas. *Elsevier Oceanography Series*, *57*, 157–181. https://doi.org/10.1016/S0422-9894(08)70066-7

Gaspar, P., Grégoris Y., & Lefevre, J. M. (1990). A simple eddy kinetic energy model for simulations of the oceanic vertical mixing: Tests at station papa and long-term upper ocean study site. *Journal of Geophysical Research*, *95*, 16,179–16,193.

Giordani, H., Lebeaupin-Brossier, C., & Léger, F. (2017). A PV-approach for dense water formation in fronts: Application to North-western Mediterranean. *Journal of Geophysical Research: Oceans*, *122*, 995–1015. https://doi.org/10.1002/2016JC012019

Grant, A. L. M. (2001). Cloud-base fluxes in the cumulus-capped boundary layer. *Quarterly Journal of the Royal Meteorological Society*, *127*, 407–421.

Gregory, D. (2001). Estimation of entrainment rate in simple models of convective clouds. *Quarterly Journal of the Royal Meteorological Society*, *127*, 53–72.

Holland, W. R. (1979). The general circulation of the ocean and its modeling. *Dynamics of Atmospheres and Oceans*, *3*, 111–142.

Houpert, L., Durrieu de Madron, X., Testor, P., Bosse, A., D'Ortenzio, F., Bouin, M. N., et al. (2016). Observations of open-ocean deep convection in the northwestern Mediterranean Sea: Seasonal and interannual variability of mixing and deep water masses for the 2007-2013 Period. *Journal of Geophysical Research: Oceans*, *121*, 8139–8171. https://doi.org/10.1002/2016JC011857

Ilicak, M., Adcroft, A. J., & Legg, S. (2014). A framework for parameterization of heterogeneous ocean convection. *Ocean Modelling*, *82*, 1–14.

Iudicone, D., Rogers, K. B., Stendardo, I., Aumont, O., Madec, G., Bopp, L., et al. (2011). Water masses as a unifying framework for understanding the Southern Ocean Carbon Cycle. *Biogeosciences*, *8*(5), 1031–1052. https://doi.org/10.5194/bg-8-1031-2011

Killworth, P. D. (1989). Parameterization of small-scale processes. In H. Winter workshop, (Ed.), *On the parameterization of deep convection in ocean models*. University of Hawaii at Manoa.

Kuo, H. L. (1974). Further Studies of the Parameterization of the Influence of cumulus Convection on Large-Scale Flow. *Journal of the Atmospheric Sciences*, *31*, 1232–1240.

Lapeyre, G., & Klein, P. (2006). Impact of the small-scale elongated filaments on the oceanic vertical pump. *Journal of Marine Research*, *64*, 835–851.

Large, W. G. (1998). Modeling and parameterization ocean planetary boundary layers. In E. P. Chassignet, & J. Verron (Eds.), *Ocean Modeling and Parameterization* (pp. 81–120). kluwer academic publishers.

Large, W. G., McWilliams, J. C., & Doney, S. (1994). Ocean vertical mixing: A review and a model with nonlocal boundary layer parameterization. *Reviews of Geophysics*, *32*, 363–403.

Lazar, A., Madec, G., & Delecluse, P. (1999). The deep interior downwelling in the Veronis effect, and mesoscale tracer transport parameterizations in an OGCM. *Journal of Physical Oceanography*, *29*, 2945–2961.

Leaman, K. D., & Schott, F. (1991). Hydrographic structure of the convection regime in the gulf of lions: Winter 1987. *Journal of Physical Oceanography*, *21*, 575–597.

Lebeaupin, C., Arsouze, T., Béranger, K., Bouin, M.-N., Bresson, E., Ducrocq, V., et al. (2014). Ocean Mixed Layer Responses to intense meteorological events during HyMeX-SOP1 from a high-resolution ocean simulation. *Ocean Modelling*, *84*, 84–103. https://doi.org/10.1016/j.ocemod.2014.09.009

Léger, F., Brossier, C. L., Giordani, H., Arsouze, T., Beuvier, J., Bouin, M. N., et al. (2016). Dense Water Formation in the North-Western Mediterranean area during HyMeX-SOP2 in 1/36° ocean simulation: Sensitivity to initial conditions. *Journal of Geophysical Research: Oceans*, *121*, 5549–5569. https://doi.org/10.1002/2015JC011542

Léger, J., Lafore, J. P., Piriou, J. M., & Guérémy, J. F. (2019). A simple Model of Convective Drafts Accounting for the Perturbation Pressure Term. *Journal of the Atmospheric Sciences*, *76*, 3129–3149.

Lellouche, J. M., Greiner, E., Galloudec, O. L., Garric, G., Regnier, C., Drevillon, M., et al. (2018). Recent updates to the Copernicus Marine Service global ocean monitoring and forecasting real-time 1/12° high-resolution system. *Ocean Science*, *14*, 1093–1126. https://doi.org/10.5194/os-14-1093-2018

Lévy, M., Ferrari, R., Franks, P. J. S., Martin, A. P., & Rivière, P. (2012). Bringing physics to life at the sub-mesoscale. *Geophysical Research Letters*, *39*, L14602. https://doi.org/10.1029/2012GL052756

MEDOC-Group (1970). Observations of formation of deep-water in the mediterranean sea. *Nature*, *227*, 1037–1040.

Madec, G., Chartier, M., & Crépon, M. (1991). Effect of thermohaline forcing variability on deep water formation in the northwestern mediterranean sea—A high resolution three-dimensional study. *Dynamics of Atmospheres and Oceans*, *15*, 301–332.

Madec, G., Chartier, M., Delecluse, P., & Crépon, M. (1991). A three-dimensional numerical studies of Deep-Water Formation in the Northwestern Mediterranean Sea. *Journal of Physical Oceanography*, *21*, 1349–1371.

Madec, G., & NEMO System Team (2016). Scientific notes of climate modelling center. In *NEMO Ocean Egine. Note du Pôle de Modélisation, Institut Pierre Simon Laplace (IPSL), France. P ublisher = Zenodo*. https://doi.org/10.5281/zenodo.1464816

Mailhôt, J., & Benoit, R. (1982). A finite-element model of the atmospheric boundary layer suitable for use with numerical weather prediction models. *Journal of the Atmospheric Sciences*, *39*, 2249–2266.

Marshall, D., & Schott, F. (1999). Open-ocean convection: Observations, theory, and models. *Reviews of Geophysics*, *37*(1), 1–64. https://doi.org/10.1029/98RG02739

Martin, V., Marshall, J., & Jones, H. (1996). Dynamics of Isolated Convective Regions in the Ocean. *Journal of Physical Oceanography*, *26*, 1721–1734.

Martin, T., Park, W., & Latif, M. (2013). Multi-centennial variability controlled by Southern Ocean convection in the Kiel Climate Model. *Climate Dynamics*, *40*(7-8), 2005–2022. https://doi.org/10.1029/2006GL026267

Mellor, G. L., & Durbin, P. A. (1975). The structure and dynamics of the ocean mixed layer. *Journal of Physical Oceanography*, *5*, 718–728.

Mellor, G. L., & Yamada, T. (1982). Development of a turbulence closure model for geophysical fluid problems. *Reviews of Geophysics*, *20*, 851–855.

Mertens, C., & Schott, F. (1998). Interannual variability of deep convection in the northwestern mediterranean. *Journal of Physical Oceanography*, *28*, 1410–1424.

Moeng, C., & Wyngaard, J. C. (1988). Spectral analysis of large-eddy simulations of the convective boundary layer. *Journal of the Atmospheric Sciences*, *45*(23), 3573–3587.

Moore, G. W. K., Vage, K., Pickart, R. S., & Renfrew, I. A. (2015). Decreasing intensity of open-ocean convection in the Greenland and Iceland seas. *Nature*, *5*, 877–882. https://doi.org/10.1038/NCLIMATE2688

Nordeng, T. E. (1994). Extended versions of the convective parametrization scheme at ECMWF and their impact on the mean and transient activity of the model in the tropics (Tech. Rep.). Reading, UK: ECMWF.

Paluszkiewicz, T., & Romea, R. D. (1997). A one-dimensional plume model for the parameterization of oceanic deep convection. *Dynamics of Atmospheres and Oceans*, *26*, 95–130.

Pergaud, J., Masson, V., Malardel, S., & Couvreux, F. (2009). A Parameterization of Dry Thermals and Shallow Cumuli for Mesoscale Numerical Weather prediction. *Boundary-Layer Meteorology*, *132*, 83. https://doi.org/10.1007/s10546-009-9388-0

Piron, A., Thierry, V., Mercier, H., & Caniaux, G. (2016). Argo float observations of basin-scale deep convection in the irminger sea during winter 2011-2012. *Deep Sea Research*, *109*, 76–90. https://doi.org/10.1016/j.dsr.2015.12.012

Reffray, G., Bourdallé-Badie, R., & Calone, C. (2015). Modelling turbulent vertical mixing sensitivity using a 1-D version of NEMO. *Geoscientific Model Development*, 5249–5293. https://doi.org/10.5194/gmdd-7-5249-2014

Rio, C., & Hourdin, F. (2008). A Thermal Plume Model for the Convective Boundary Layer: Representation of Cumulus Clouds. *Journal of the Atmospheric Sciences*, *65*, 407–425. https://doi.org/10.1175/2007JAS2256.1

Rio, C., Hourdin, F., Couvreux, F., & Jam, A. (2010). Resolved versus parametrized Boundary-Layer plumes. part II: Continuous formulations of mixing rates for Mass-Flux schemes. *Boundary-Layer Meteorology*, *135*, 469–483. https://doi.org/10.1007/s10546-010-9478-z

Rodi, W. (1987). Examples of calculation methods for flow and mixing in stratified fluids. *Journal of Geophysical Research*, *92*, 5305–5328.

Sander, J., Wolf-Gladrow, D., & Olbers, D. (1995). Nnumerical studies of open ocean deep convection. *Journal of Geophysical Research*, *100*, 20,579–20,600.

Siebesma, A. P. (1998). Shallow cumulus convection. In E. J. Plate, E. E. Fedorovich, D. X. Viegas, & J. C. Wyngaard (Eds.), *Buoyant convection in geophysical flow* (pp. 441–486). kluwer acad. publishers.

Siebesma, A. P., Bretherton, C. S., Brown, A., Chlond, A., Cuxart, J., Duynkerke, P. G., et al. (2003). A large eddy simulation intercomparison study of shallow cumulus convection. *Journal of the Atmospheric Sciences*, *60*, 1201–1219.

Siebesma, A. P., & Cuijpers, J. W. M. (1995). Evaluation of Parametric Assumptions for Shallow Cumulus Convection. *Journal of the Atmospheric Sciences*, *52*, 650–666.

Siebesma, A., & Teixeira J. (2000). An advection-diffusion scheme for the convective boundary layer, description and 1D results. In *Proceedings of 14th AMS Symposium on Boundary Layers and Turbulence*, AMS.

Simpson, J., & Wiggert, V. (1969). Mmodels of precipitating cumulus towers. *Monthly Weather Review*, *97*, 471–489.

Skyllingstad, E. D., Denbo, D. W., & Downing, J. (1991). Convection in the Labrador Sea: Community modeling effort results. In P. Chu, & J. C. Gascard (Eds.), *Deep Convection and Deep Water Formation in the Oceans* (pp. 341–354). Amsterdam: Elsevier.

Smith, N. R. (1989). The southern ocean thermohaline circulation: A numerical model sensitivity study. *Journal of Physical Oceanography*, *23*, 713–726.

Soares, P., Miranda, P., Siebesma, A., & Teixeira, J. (2004). An eddy-diffusivity/mass-flux parametrization for dry and shallow cumulus convection. *Quarterly Journal of the Royal Meteorological Society*, *130*, 3365–3383.

Somot, S., Houpert, L., Sevault, F., Testor, P., Bosse, A., Taupier-Letage, I., et al. (2016). Characterizing, modelling and understanding the climate variability of the deep water formation in the north-western mediterranean sea. *Climate Dynamics*, *28*, 1–32.

Steffen, E., & D'Asaro, E. (2002). Deep Convection in the Labrador Sea as Observed by Lagrangian Floats. *Journal of Physical Oceanography*, *32*, 475–492. https://doi.org/10.1175/1520-0485(2002)032

Storto, A., Masina, S., & Simoncelli, S. (2019). The added value of the multi-system spread information for ocean heat content and steric sea level investigations in the CMEMS GREP ensemble reanalysis product. *Climate Dynamics*, *53*, 287–312. https://doi.org/10.1007/s00382-018-4585-5

Stössel, A., Yang, K., & Kim, S. J. (2002). On the Role of Sea Ice and Convection in a Global Ocean Model. *Journal of Physical Oceanography*, *32*, 1194–1208.

Stull, R. B. (2003). *An Introduction to Boundary Layer Meteorology* (pp. 666). Kluwer Academic Publishers.

Suselj, K., Kurowski, M. J., & Teixeira, J. (2019). A unified eddy-diffusivity/mass-flux approach formodelin atmospheric convection. *Journal of the Atmospheric Sciences*, *76*, 2505–2537. https://doi.org/10.1175/JAS-D-18-0239.1

THETIS-Group (1994). Open-Ocean deep convection explored in the mediterranean. *EOS, Transactions American Geophysical Union*, *75*(19), 219–221.

Testor, P., Bosse, A., Houpert, L., Margirier, F., Mortier, L., Legoff, H., et al. (2018). Multiscale observations of deep convection in the northwestern mediterranean sea during winter 2012-2013 using multiple platforms. *Journal of Geophysical Research: Oceans*, *123*, 1745–1776. https://doi.org/10.1002/2016JC012671

Thomas, L. N., & Ferrari, R. (2008). Friction, Frontogenesis, and the Stratification of the Surface Mixed-Layer. *Journal of Physical Oceanography*, *38*, 2501–2518.

UNESCO (1981). The Practical Salinity Scale 1978 and the International Equation of State of Seawater. *UNESCO Technical Papers in Marine Science*, *36*, 25.

Umlauf, L., & Burchard, H. (2003). A generic lengh-scale equation for geophysical turbulence models. *Journal of Marine Research*, *61*, 235–265. https://doi.org/10.1357/002224003322005087

Wang, S., & Stevens, B. (2000). Top-hat representation of turbulence statistics topped boundary-layers: A large-eddy simulation study. *Journal of the Atmospheric Sciences*, *57*, 423–441.

Wilcox, D. C. (1988). Reassessment of the scale-determining equation for advanced turbulence models. *AIAA Journal*, *26*, 1299–1310.